Caffeinated Interfaces Enhance Alkaline Hydrogen Electrocatalysis

Saad Intikhab[1], Luis Rebollar[1], Yawei Li[1], Rahul Pai[1], Vibha Kalra[1], Maureen Tang[1], Joshua Snyder[1]*

[1] *Department of Chemical and Biological Engineering, Drexel University, Philadelphia, PA 19104*

**Corresponding author: jds43@drexel.edu*

Abstract

The high Pt loading required for hydrogen oxidation (HOR) and evolution (HER) reactions in alkaline fuel cells and electrolyzers adversely impacts the system cost. Here, we demonstrate the use of caffeine as a 'double-layer dopant' to enhance both the HER and HOR of Pt electrodes in base. HER/HOR rates increase by fivefold on Pt(111) and are accelerated on Pt(110), Pt(pc), and Pt/C as well. FTIR spectroscopy confirms that caffeine is adsorbed at the Pt surface, forming a self-limiting film through electrochemical deposition. Caffeine films are stable up to 1.0 V vs. RHE and are readily regenerated through caffeine deposition during load/potential cycling. The findings presented here both identify a potential catalyst additive that can mitigate high Pt loadings in alkaline fuel cells and electrolyzers while opening the door to molecular engineering of solid/liquid interfaces for energy storage and conversion.

Introduction

The hydrogen evolution and oxidation reactions (HER/HOR) remain two of the most fundamental reactions in electrochemistry. Despite decades of research, the source of the pH dependence of HER/HOR kinetics remains controversial[1–8]. Both reactions are several orders of magnitude slower in alkaline compared to acidic electrolytes, even on Pt. This performance disparity necessitates higher Pt loadings in alkaline fuel cells (AFC) and electrolyzers, adversely impacting system cost. Further commercial advancement of these high pH devices requires a generational advancement in catalyst technology to drive reduction in precious metal loadings.

Rational electrocatalyst design at alkaline pH requires a fundamental understanding of the anomalous pH dependence. Several different schools of thought have evolved over the past decade

to explain the slower catalytic rates at alkaline pH. An emerging consensus has recognized that hydrogen binding energy (HBE) cannot be the sole activity descriptor in base, and many inconsistencies have been found in the HBE argument[9–11]. Markovic et al. proposed the so-called 'bifunctional theory' which states that in base, both optimal H and OH binding are necessary for improved HER/HOR[12–15]. We have showed in our previous works that OH_{ad} is not an active participant in the hydrogen reactions and any effect it has on HER/HOR kinetics may be indirect[16–18]. Another prominent school of thought hypothesizes that the electrostatic interaction of water dipoles with the electric field influences water reorganization kinetics and can explain the pH dependence[9,19,20]. While there is good evidence that the electric field is stronger at high pH than at low pH, a direct link between field strength and water dynamics remains to be proven.

Despite disagreements on the molecular origin of HER/HOR kinetics in base, researchers agree that interfacial water structure is critical[6,9,21–23]. In other words, next-generation electrocatalysts must engineer not only intermediate adsorption energies, but also the electrochemical double-layer structure and dynamics. While the complexity of this task is daunting, literature already provides many examples where manipulating solution structure enhances electrocatalytic rates. In alkaline HER/HOR, cation effects provide a simple demonstration of this approach[7,24,25]. More nuanced effects can be realized with ionic liquid electrolytes in the carbon dioxide reduction reaction (CO_2RR) and oxygen reduction reaction (ORR)[26–28]. These and other examples have recognized that the electrolyte, in addition to the electrode, provides opportunities to direct chemical transformations.

In this work, we demonstrate the efficacy of the "double-layer dopant" approach with the molecular additive caffeine. As a hydro- and oxo-phobic molecule, caffeine can inhibit corrosion by preventing oxygen molecules and water from interacting with the electrode surface[29]. While it is hydrophobic, it is slightly polar and is known to affect the hydrogen bonding network and mobility of surrounding water molecules[30,31]. Molecular dynamics simulations, in the absence of an electric field, show that water structures in a complex fashion around the planar caffeine molecules[30]. In this work, we show that electrochemically deposited caffeine 'films' on Pt surfaces yield HER/HOR rate enhancements greater than 5X in alkaline electrolyte. The impact of caffeine on the reversible hydrogen kinetics exhibits a strong structural sensitivity to the atomic geometry of the underlying Pt surface as well as marked change in effect with electrolyte pH. Preliminary

insight into the source of the activity enhancement at alkaline pH suggests that caffeine affects interfacial water in the double layer to facilitate lower transition-state barriers at high pH.

Figure 1(a) shows the HER/HOR polarization curves for Pt(111) in 0.1 M KOH with and without caffeine (10^{-4} M) in solution. Caffeine significantly reduces the overpotential for HER at 10 mA/cm^2 by ~155 mV and for HOR at 1 mA/cm^2 by ~96 mV, while maintaining a similar diffusion-limited current density. Exchange current densities normalized by electrochemically active surface area (ECSA) are listed in **Table 1**. Throughout this work, geometric current density is reported as mA/cm^2 and ECSA-normalized current density is reported as mA/cm$^2_{Pt}$. The negligible impact to the diffusion limited current is counterintuitive, based on **Figure 1(b)**. The adsorbed caffeine appears to block active sites on the Pt surface, as evidenced by the decrease in charge associated with hydrogen underpotential deposition (H_{UPD}**)**. Supplementary **Figure S1** shows how varying the concentration of caffeine in solution affects the polarization curves. Increasing the concentration of caffeine in the electrolyte beyond 10^{-4} M does not result in any further change to the HER/HOR polarization curves. **Figure S2** shows a gradual decay in H_{UPD} and OH_{ad} charge on Pt(111) as the potential is cycled in a solution containing caffeine. The rate of feature decay is a function of the concentration of caffeine in solution. With continued potential cycling, the CV features eventually stop decreasing and the corresponding HER/HOR performance stagnates. The absence of any further increase or even decrease in HER/HOR activity points to a self-limiting formation of a caffeine film on the electrode surface. At a steady-state coverage, no further increase in faradaic feature decrease with cycle number, integration of the currents in the electrochemical H_{UPD} and $OH_{ads/des}$ regions indicate a decrease in charge by 35% and 56% respectively. **Figure 1(d)** is an ex-situ FTIR spectra of a caffeine film on Pt(pc) following electrochemical deposition and subsequent rinsing with DI water. After deposition, the caffeine film is stable on the surface and still improves HER/HOR activity after transfer to an electrolyte that does not contain caffeine, see **Figures 1** and **S3**. Oxidative cycling in **Figure S4** shows that caffeine films are stable up to potentials of 1.0 V vs. RHE. Beyond this potential, the caffeine film is slowly removed from the surface through oxidation, eventually yielding the HER/HOR activity of the bare Pt electrode. With caffeine present in the electrolyte, the caffeine film is readily regenerated during potential cycling between 0 and 0.9 V vs. RHE, **Figure S4**. The ability to transfer activity to a caffeine-free electrolyte and to regenerate the film once oxidatively removed when caffeine is present in the electrolyte points to the utility of caffeine as a catalyst additive. For

example, during startup and shutdown, the cathode and anode of water electrolyzers and fuel cells, respectively, can experience potentials greater than 1.0 V vs. RHE. If caffeine were integrated into such a device, films removed during startup/shutdown events could be readily reformed through exposure to a doped electrolyte. The impact of caffeine on HER/HOR in alkaline electrolyte is also observed on more defected surfaces including Pt (110) and polycrystalline Pt (Pt(pc)), **Figure 2(a)** and **2(c)**. For Pt(pc), the exchange current densities (i_o) improve from 0.30 mA/cm^2 (0.38 mA/cm$^2_{Pt}$) to 0.86 mA/cm^2 ((2.84 mA/cm$^2_{Pt}$))whereas for Pt(110), the exchange current densities (i_o) improve from 1.03 mA/cm^2 (1.01 mA/cm$^2_{Pt}$) to 2.21 mA/cm^2 (6.22 mA/cm$^2_{Pt}$). On Pt(110) and Pt(pc), the HOR current begins to decay at potentials above ~0.6 V vs. RHE. This decay can be ascribed to the competitive adsorption of H_2 and OH_{ad} where the surface coverage of spectator OH_{ad} at the higher potentials lowers the density of active sites. In the presence of the caffeine film, a significant recovery in the HOR current density is observed at higher potentials, **Figure 2(a)**. We potentially ascribe this recovery to caffeine's association with lower coordinated defect sites or decreasing the OH_{ad} binding energy. In the CVs in **Figure 2(b)**, H_{UPD} features are suppressed in the presence of caffeine for both Pt(110) and Pt(pc), which have been associated with an H/OH exchange on lower coordinated sites[10,11,16,32]. A similar loss in H/OH exchange charge is observed from a Pt(111) surface onto which low coordinated Pt-adislands have been deposited[12], **Figure S5**. The direct association of caffeine with lower coordinated defects is observed during deposition of the caffeine film where H/OH features associated with (110)/(100)-like defects rapidly disappear at early times, **Figure S5**. Extension of the diffusion limited HOR current density to higher potentials has also been observed for nanoscale catalysts, Pt/C, as shown in **Figure S6**. The effect of caffeine on OH adsorption is more directly observed by analyzing its effect on reactions where OH_{ad} is a demonstrated reactant[33], namely CO oxidation. **Figures 2(d) and S7** show that caffeine causes a positive shift in the peak and onset potentials for CO bulk oxidation and CO monolayer stripping, respectively. Together, **Figures 1, 2 and S7** indicate that the presence of caffeine on the surface reduces the coverage of spectator OH_{ad} species, either through a physical competition for adsorption sites or through a weakening of the interaction between the Pt surface and OH_{ad}. Further work is needed to discern which of these effects is greater.

The impact of caffeine on HER/HOR kinetics is surprising and the source of this activity enhancement remains an open question. In addition to the decay in H_{UPD} and OH_{ad} coverage, as determined through integration of the corresponding features in the CVs in **Figures 1(b)**, a

measurable shift in the H adsorption threshold towards less positive potentials is observed, indicating either weakening of HBE or a possible decrease in H_{ad}-H_{ad} repulsion with a decrease in H_{ad} coverage[34–36]. Additionally, a positive shift in the onset potential for the formation of OH_{ad}, **Figure 1(b)**, points to a potential weakening of OH_{ad} binding in the presence of the caffeine film. However, several groups have recently highlighted the fact that thermodynamic adsorption energies alone are insufficient to fully describe the HER/HOR kinetics at alkaline pH[9,16,17,19,20]. If caffeine is weakening the HBE, as indicated by the negative shift in the H_{UPD} onset threshold on Pt(111) (**Figure 1(b)**), and the improved HER/HOR kinetics were a direct result of the weakened HBE, a similar result would be expected in acid. As shown in **Figure 3**, caffeine on Pt(111) results in a decrease in HER/HOR activity at pH 1, **Figure 3(a)**, while maintaining a similar shift in H_{UPD} threshold potential, **Figure 3(b)**. While oxophilic sites on a Pt surface have been implicated in a beneficial bifunctional mechanism[15], we have previously argued that OH_{ad} is not an active participant in the reaction and must be improving the reaction kinetics indirectly[16–18]. In line with that work, here it is found that adsorbed caffeine on a Pt surface increases HER/HOR activity at alkaline pH, while at the same time weakening OH binding energy and reducing the oxophilicity of the surface, **Figure 1, 2,** and **S7**. While the direct mechanistic impact of interfacial caffeine on the HER/HOR kinetics is not yet fully understood, future work to gain further insight will be guided by current understanding of pH effects in the reversible hydrogen reaction. It is likely that the thin caffeine film on the surface of Pt disrupts the double layer structure to directly affect the water orientation and dynamics. It has been proposed that at high pH, the stronger electric field at a given potential induces rigidity in the near surface water, lowering reorganization kinetics and impeding charge transfer[9,19,20]. Caffeine at the metal/electrolyte interface may improve alkaline HER/HOR kinetics by weakening the electric field near reversible hydrogen potential, making water reorganization more facile. This interpretation would be supported by the observed behavior at pH 1, **Figure 3**. The electric field is already weak in acid near the reversible hydrogen potential and water reorganization kinetics are not expected to play a role in defining the overall reaction rate[20,37–39]. The addition of caffeine to the interface would then just act to block active sites, yielding a decrease in activity. Efforts to understand how caffeine affects the water in the double layer are ongoing.

In summary, we have shown how caffeine as a ‘double layer dopant’ can enhance the catalytic activity of Pt surfaces in alkaline medium. The most significant improvement is seen for

the Pt(111) surface where the HER current densities are ~7 times higher and HOR current densities are ~5 times higher at 100 mV overpotential. The improvement in HER and HOR is also seen for Pt(110), Pt(pc) and commercial Pt/C where the exchange current densities are enhanced by 2.2 times, 2.9 times and 1.4 times respectively. FTIR spectroscopy shows that caffeine is specifically adsorbed on the Pt surface and our results suggest that adsorbed caffeine weakens OH binding energy and possibly affects the water dynamics in the double layer. While the specific source of the activity enhancement may not be definitively identified, our preliminary insights based on the observed results might have implications on understanding the pH dependence of reversible hydrogen reactions. Molecular double layer dopants present the opportunity to push beyond the activity of standard catalysts, where a nearly infinite library of additive chemistries highlight the potential of this approach for significant impact.

Table 1: ECSA values calculated for bare Pt(111) and Pt(111)+caffeine measured by H_{UPD} and CO stripping and correspondingly normalized HER/HOR exchange current densities.

	ECSA (H_{UPD}) (cm^2_{Pt}/cm^2_{geo})	Exchange Current Density (i_o; $mA/cm^2_{Pt(HUPD)}$)	ECSA (CO stripping) (cm^2_{Pt}/cm^2_{geo})	Exchange Current Density (i_o; $mA/cm^2_{Pt(CO)}$)
Pt(111) – 0.1 M KOH	0.45	0.08	0.57	0.06
Pt(111) + caffeine – 0.1 M KOH	0.29	0.61	0.38	0.48
Pt(111) – 0.1 M $HClO_4$	0.56	3.31	0.77	2.38
Pt(111) + caffeine – 0.1 M $HClO_4$	0.26	1.86	0.43	1.12

Acknowledgements

SI, LR, MHT, and JDS acknowledge support from NSF CBET-Catalysis 1602886.

References

(1) Bagotsky, V. S.; Osetrova, N. V. *Electroanal. Chem. Interfacial Electrochem.* **1973**, *43*, 233–249.

(2) Marković, N. M.; Sarraf, S. T.; Gasteiger, H. A.; Ross, P. N. *J. Chem. Soc. Faraday Trans.* **1996**, *92* (20), 3719–3725.

(3) Sheng, W.; Gasteiger, H. A.; Shao-Horn, Y. *J. Electrochem. Soc.* **2010**, *157* (11), B1529.

(4) Zheng, J.; Zhuang, Z.; Xu, B.; Yan, Y. *ACS Catal.* **2015**, *5* (7), 4449–4455.

(5) Zheng, J.; Nash, J.; Xu, B.; Yan, Y. *J. Electrochem. Soc.* **2018**, *165* (2), H27–H29.

(6) Liu, E.; Li, J.; Jiao, L.; Thi, H.; Doan, T.; Liu, Z.; Zhao, Z.; Huang, Y.; Abraham, K. M.; Mukerjee, S.; Jia, Q. **2019**.

(7) Weber, D. J.; Janssen, M.; Oezaslan, M. *J. Electrochem. Soc.* **2019**, *166* (2), F66–F73.

(8) Intikhab, S.; Natu, V.; Li, J.; Li, Y.; Tao, Q.; Rosen, J.; Barsoum, M. W.; Snyder, J. *J. Catal.* **2019**, *371*, 325–332.

(9) Ledezma-Yanez, I.; Wallace, W. D. Z.; Sebastián-Pascual, P.; Climent, V.; Feliu, J. M.; Koper, M. T. M. *Nat. Energy* **2017**, *2* (4), 1–7.

(10) Chen, X.; McCrum, I. T.; Schwarz, K. A.; Janik, M. J.; Koper, M. T. M. *Angew. Chemie - Int. Ed.* **2017**, *56* (47), 15025–15029.

(11) McCrum, I. T.; Janik, M. J. *J. Phys. Chem. C* **2016**, *120* (1), 457–471.

(12) Subbaraman, R.; Tripkovic, D.; Strmcnik, D.; Chang, K.-C.; Uchimura, M.; Paulikas, A. P.; Stamenkovic, V. R.; Marković, N. M. *Science (80-.).* **2011**, *334* (December), 1256–1260.

(13) Strmcnik, D.; Uchimura, M.; Wang, C.; Subbaraman, R.; Danilovic, N.; van der Vliet, D.; Paulikas, A. P.; Stamenkovic, V. R.; Markovic, N. M. *Nat. Chem.* **2013**, *5* (4), 300–306.

(14) Danilovic, N.; Subbaraman, R.; Strmcnik, D.; Chang, K.-C.; Paulikas, A. P.; Stamenkovic, V. R.; Marković, N. M. *Angew. Chemie* **2012**, *51* (50), 12495–12498.

(15) Subbaraman, R.; Tripkovic, D.; Chang, K. C.; Strmcnik, D.; Paulikas, A. P.; Hirunsit, P.; Chan, M.; Greeley, J.; Stamenkovic, V.; Markovic, N. M. *Nat. Mater.* **2012**, *11* (6), 550–557.

(16) Intikhab, S.; Snyder, J. D.; Tang, M. H. *ACS Catal.* **2017**, *7* (12), 8314–8319.

(17) Rebollar, L.; Intikhab, S.; Snyder, J. D.; Tang, M. H. *J. Electrochem. Soc.* **2018**, *165* (15), in press.

(18) Intikhab, S.; Rebollar, L.; Fu, X.; Yue, Q.; Li, Y.; Kang, Y.; Tang, M. H.; Snyder, J. D. *Nano Energy* **2019**, *64* (August), 103963.

(19) Sarabia, F. J.; Sebastián-Pascual, P.; Koper, M. T. M.; Climent, V.; Feliu, J. M. *ACS Appl. Mater. Interfaces* **2019**, *11* (1), 613–623.

(20) Ryu, J.; Surendranath, Y. *J. Am. Chem. Soc.* **2019**, *141* (39), 15524–15531.

(21) Liu, Ershuai; Jiao, Li; Li, Jingkun; Stracensky, Thomas; Richard, Lynne Larochelle; Sun, Qiang; Mukerjee, Sanjeev; Jia, Q. ChemRxiv **2019**.

(22) Dubouis, N.; Grimaud, A. *Chem. Sci.* **2019**, *10* (40), 9165–9181.

(23) Zeradjanin, A. R.; Vimalanandan, A.; Polymeros, G.; Topalov, A. A.; Mayrhofer, K. J. J.; Rohwerder, M. *Phys. Chem. Chem. Phys.* **2017**, *19* (26), 17019–17027.

(24) Strmcnik, D.; Kodama, K.; van der Vliet, D.; Greeley, J.; Stamenkovic, V. R.; Marković, N. M. *Nat. Chem.* **2009**, *1* (6), 466–472.

(25) Chung, H. T.; Choe, Y. K.; Martinez, U.; Dumont, J. H.; Mohanty, A.; Bae, C.; Matanovic, I.; Kim, Y. S. *J. Electrochem. Soc.* **2016**, *163* (14), F1503–F1509.

(26) Kumeda, T.; Tajiri, H.; Sakata, O.; Hoshi, N.; Nakamura, M. *Nat. Commun.* **2018**, *9* (1).

(27) Snyder, J.; Fujita, T.; Chen, M. W.; Erlebacher, J. *Nat. Mater.* **2010**, *9* (11), 904–907.

(28) Faggion, D.; Gonçalves, W. D. G.; Dupont, J. *Front. Chem.* **2019**, *7* (MAR), 1–8.

(29) De Souza, F. S.; Giacomelli, C.; Gonçalves, R. S.; Spinelli, A. *Mater. Sci. Eng. C* **2012**, *32* (8), 2436–2444.

(30) Tavagnacco, L.; Schnupf, U.; Mason, P. E.; Saboungi, M. L.; Cesàro, A.; Brady, J. W. *J. Phys. Chem. B* **2011**, *115* (37), 10957–10966.

(31) Smit, W. J.; van Dam, E. P.; Cota, R.; Bakker, H. J. *J. Phys. Commun.* **2019**, *3* (2), 025010.

(32) Van Der Niet, M. J. T. C.; Garcia-Araez, N.; Hernández, J.; Feliu, J. M.; Koper, M. T. M. *Catal. Today* **2013**, *202* (1), 105–113.

(33) Li, Y.; Hart, J.; Profitt, L.; Intikhab, S.; Chatterjee, S.; Taheri, M.; Snyder, J. *ACS Catal.* **2019**, *9* (10), 9311–9316.

(34) Marković, N. M.; Grgur, B. N.; Ross, P. N. *J. Phys. Chem. B* **1997**, *5647* (97), 5405–5413.

(35) Ross, P. N. *Surface Science*. 1981, pp 463–485.

(36) Markovic, N. M.; Ross Jr., P. N. *Surf. Sci. Rep.* **2002**, *45* (4–6), 117–229.

(37) Rizo, R.; Sitta, E.; Herrero, E.; Climent, V.; Feliu, J. M. *Electrochim. Acta* **2015**, *162*, 138–145.

(38) Martínez-Hincapié, R.; Sebastián-Pascual, P.; Climent, V.; Feliu, J. M. *Russ. J. Electrochem.* **2017**, *53* (3), 227–236.

(39) Rebollar, L.; Intikhab, S.; Snyder, J. D.; Tang, M. H. *J. Phys. Chem. Lett.* **2020**, 2308–2313.

Figures

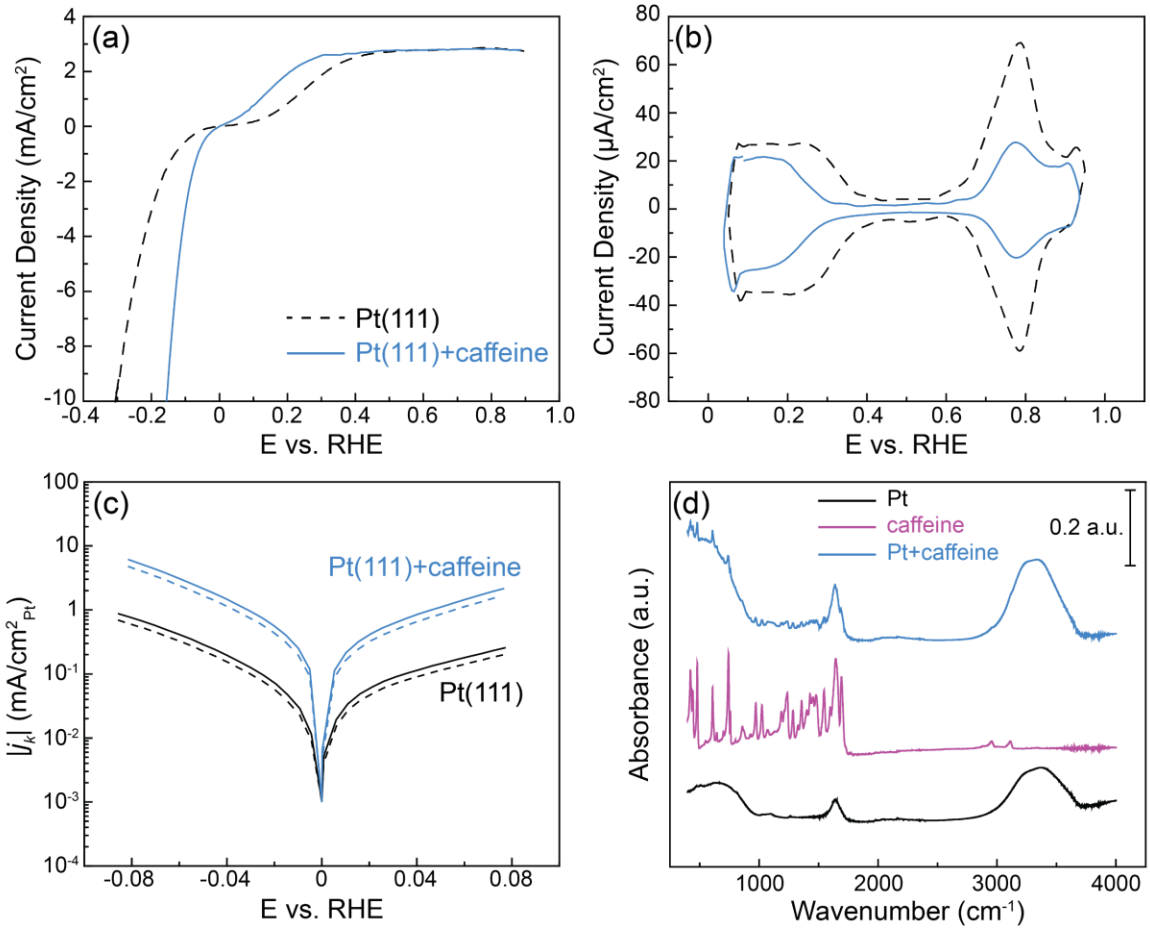

Figure 1: (a) HER/HOR polarization curves for Pt(111) (black dashed line) and Pt(111)+caffeine (blue solid line) in H_2 saturated 0.1 M KOH (anodic sweep, 50 mV/s). (b) CV of Pt(111) (black dashed line) and Pt(111)+caffeine (blue solid line) in Ar purged 0.1 M KOH. (c) Tafel plots for Pt(111) (black) and Pt(111)+caffeine (blue) (solid lines are normalized by H_{UPD} ECSA and dashed lines are normalized by CO stripping ECSA). (d) FTIR spectra of bare Pt (black), caffeine molecule (purple), and caffeine film on Pt (blue).

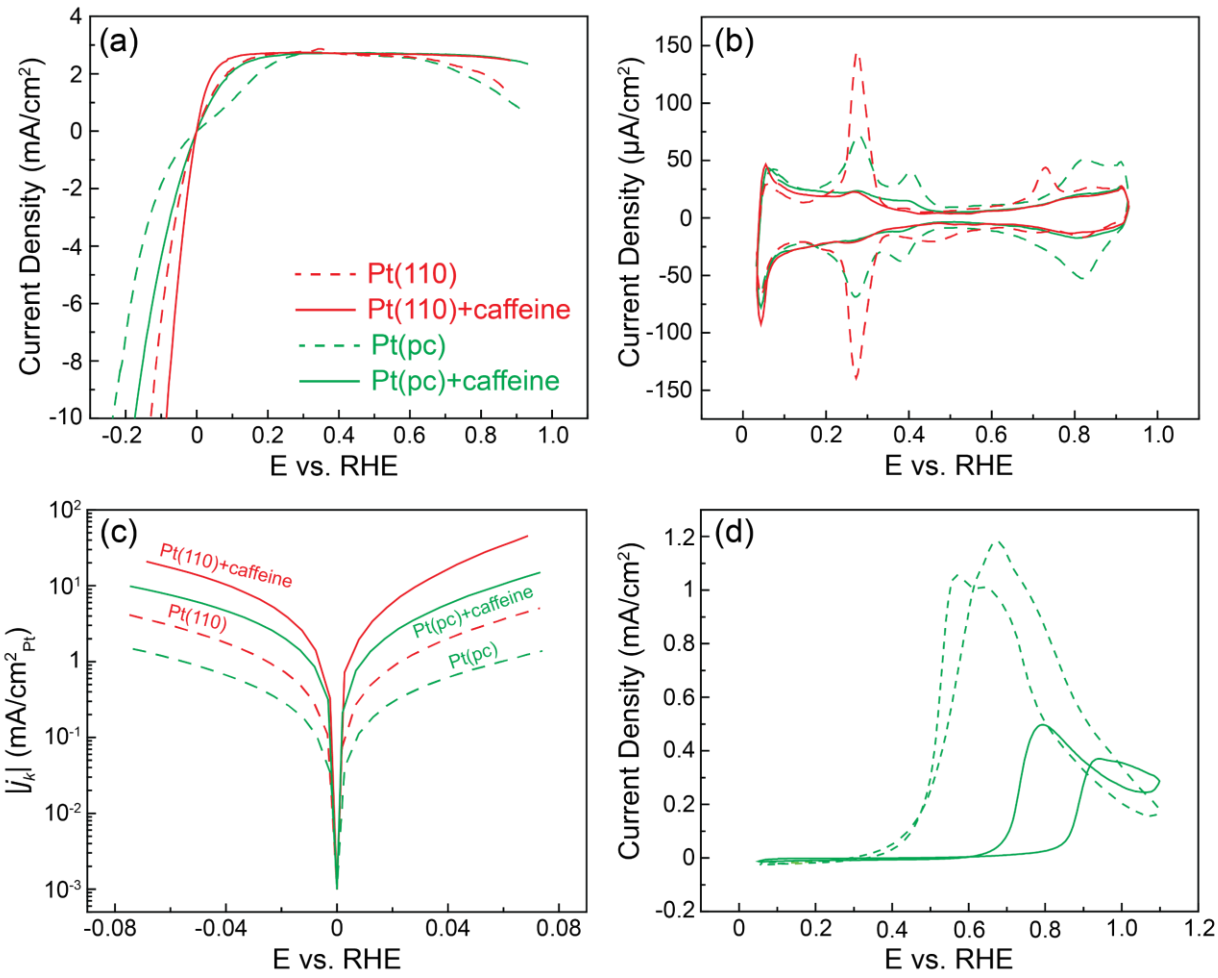

Figure 2: (a) HER/HOR polarization curves for Pt(110) (red dashed line), Pt(110)+caffeine (red solid line), Pt(pc) (green dashed line), and Pt(pc)+caffeine (green solid line) in H_2 saturated 0.1 M KOH (anodic sweep, 50 mV/s). (b) CV of Pt(110) (red dashed line), Pt(110)+caffeine (red solid line), Pt(pc) (green dashed line), and Pt(pc)+caffeine (green solid line) in Ar purged 0.1 M KOH. (c) Tafel plots generated from the corresponding polarization curves in (a). (d) CO electrooxidation on Pt(pc) (green dashed line) and Pt(pc)+caffeine (green solid line) CO saturated 0.1 M $HClO_4$, 1600 rpm.

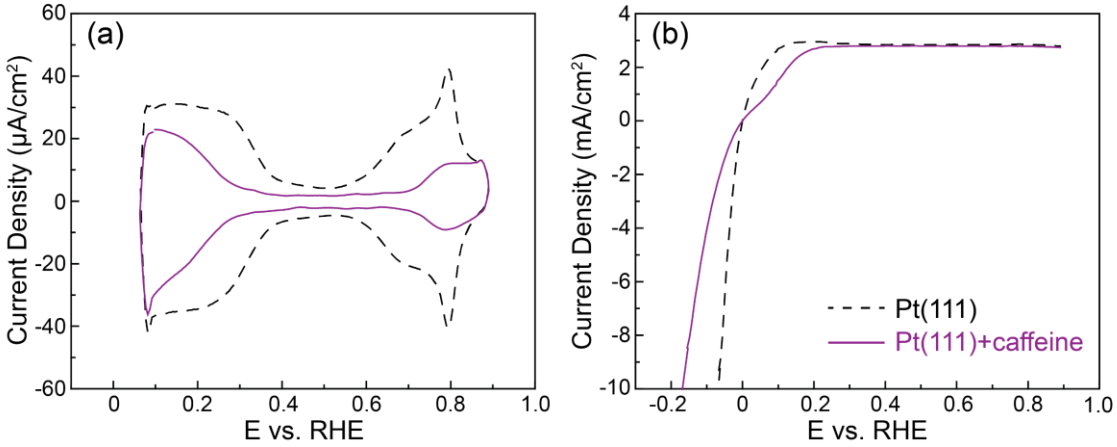

Figure 3: (a) CV of Pt(111) (black dashed line) and Pt(111)+caffeine (purple solid line) in Ar purged 0.1 M $HClO_4$. (b) HER/HOR polarization curves for Pt(111) (black dashed line) and Pt(111)+caffeine (purple solid line) in H_2 saturated 0.1 M $HClO_4$.

TOC Graphic

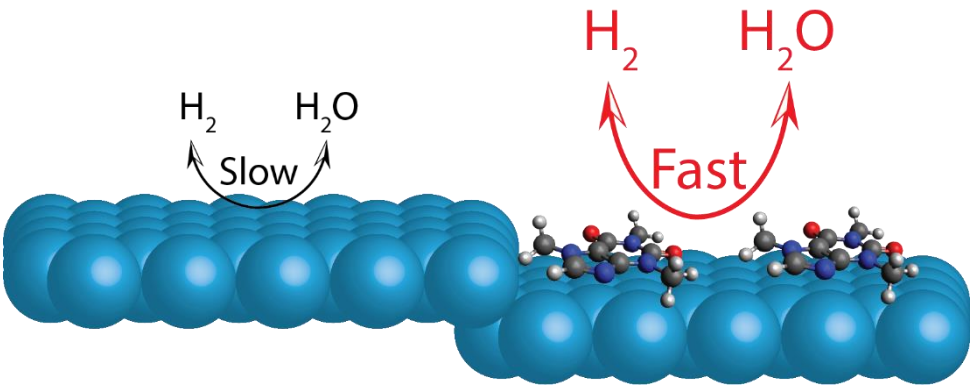

Supporting Information

Caffeinated Interfaces Enhance Alkaline Hydrogen Electrocatalysis

Saad Intikhab[1], Luis Rebollar[1], Yawei Li[1], Rahul Pai[1], Vibha Kalra[1], Maureen Tang[1], Joshua Snyder[1]*

[1] *Department of Chemical and Biological Engineering, Drexel University, Philadelphia, PA 19104*

**Corresponding author: jds43@drexel.edu*

Methods

4.1 Electrochemical Measurements

Electrochemical measurements were made at room temperature in a FEP electrochemical cell using an Autolab PGSTAT302N potentiostat with a rotating disc electrode (RDE) setup (Pine Instruments). Pt mesh (99.9%, Alfa Aesar) bonded to the end of a Pt wire (99.9%, Alfa Aesar) was used as a counter electrode. The Ag/AgCl (BASi) reference electrode was calibrated against a hydrogen reference and separated from the working electrode by an electrolyte bridge. All potentials reported in this manuscript are referenced to the reversible hydrogen electrode (RHE) and corrected for iR loss. Prior to any electrochemical experiments, the electrochemical cell and electrodes were cleaned by soaking in a solution of concentrated 1:1 H_2SO_4:HNO_3 for at least 2 hours followed by rinsing and boiling in Millipore (Milli-Q Synthesis A10) water. Electrolytes were made from high purity precursors: KOH (Sigma Aldrich, semiconductor grade, 99.99% [metal basis]), $HClO_4$ (70 wt%, Suprapur, Merck) and Millipore water (18.2 MΩ-cm, < 3 ppb TOC).

Cyclic voltammetry (CV) profiles were obtained in Ar-(research grade, Airgas) purged electrolyte with a potential range of 0.05 – 0.9 V vs. RHE at a scan rate of 50 mV/s. HER/HOR polarization curves were obtained through potential cycling between -0.3 – 0.9 V vs. RHE in H_2 saturated electrolyte at a rotation rate of 1600 rpm. All polarization curves in this paper are normalized by the geometric surface area. Experiments were repeated more than thrice in order to confirm that the results were repeatable (Figure S10-12). For the highly sensitive Pt (111) single crystal surface, two different individuals performed the experiments separately in order to confirm the consistency of results. Tafel plots are normalized by the electrochemical active surface area (ECSA) as determined by the area under the H_{upd} region/CO stripping curve for Pt (111) and H/OH exchange region for the other Pt surfaces. Kinetic current densities for HOR, used for Tafel plots and calculation of exchange current densities (i_o), were calculated using the Koutecky-Levich equation to adjust for mass transport limitations:

$$\frac{1}{i_n} = \frac{1}{i_k} + \frac{1}{i_d} \qquad \text{(Eq. 1)}$$

where, i_n is the measured current density, i_d is the diffusion-limited current density, and i_k is the kinetic current density.

The exchange current densities (i_o) are extracted from the micropolarization region (η = ± 10 mV). Butler-Volmer equation (for small overpotentials (η)) can be linearized into the form:

$$i_o(\alpha_a + \alpha_b) = \frac{RT}{F}\frac{i_n}{\eta} \qquad \text{(Eq. 2)}$$

where, α_a and α_b are anodic and cathodic transfer coefficients, F is Faraday's constant, R is the ideal gas constant, and T is temperature.

Using the linearized form of Butler-Volmer, exchange current density is calculated by multiplying the slope of the lines of the micropolarization regions, shown in Figure S13-14, by RT/F. The value of ($\alpha_a + \alpha_b$) is assumed to be 1.

4.2 Electrode preparation and caffeine deposition

Pt(111) (Princeton Scientific, 5 mm dia.), Pt(110) (Princeton Scientific, 5 mm dia.), and Pt(pc) were annealed at 1100 °C for 10 minutes under 3% H_2/Ar flow (Airgas). After cooling for 5 minutes in the same gas, the disk was protected with a drop of Millipore water, mounted in the RDE holder and transferred to the electrolyte with immersion under potential control at 0.1 V. For caffeine deposition, caffeinated electrolytes were used which were prepared by adding caffeine (>99%, Sigma Aldrich) to 60 mL of 0.1 M KOH/0.1 M $HClO_4$ to obtain concentrations of 10^{-5} M/10^{-4} M caffeine in solution. Following immersion of the prepared electrode into the Ar purged electrolyte, the potential was cycled between 0.05 – 0.9 V at 50 mV/s. The potential cycling led to the deposition of caffeine on the electrode surface as shown by the gradual suppression of CV features with each subsequent cycle (Figure S9). All CVs reported in the manuscript show the steady-state current response after deposition cycling.

CO stripping/bulk CO oxidation

The CO stripping/bulk CO oxidation measurements were completed in a FEP cell using an Autolab PGSTAT302N potentiostat in a RDE setup. The Ag/AgCl (BASi) reference electrode was used with a glass double-junction jacket to limit contamination of the working electrodes and Pt mesh was used as the counter electrode. In the CO stripping procedure, the working electrode potential was held constant at 0.2 V as CO was bubbled into the electrolyte. When the current decayed to zero due to CO passivation, CO bubbling was stopped, and the electrolyte was purged

with Ar for 20 minutes after which CO was stripped from the surface by cycling the potential to 1.1 V vs RHE. For bulk CO oxidation, the working electrode was transferred to CO purged electrolyte and the potential was cycled from 0.1 – 1.1 V. For caffeinated experiments, caffeine was deposited on the working electrodes prior to CO stripping or bulk CO oxidation measurements in uncaffeinated electrolyte.

a)

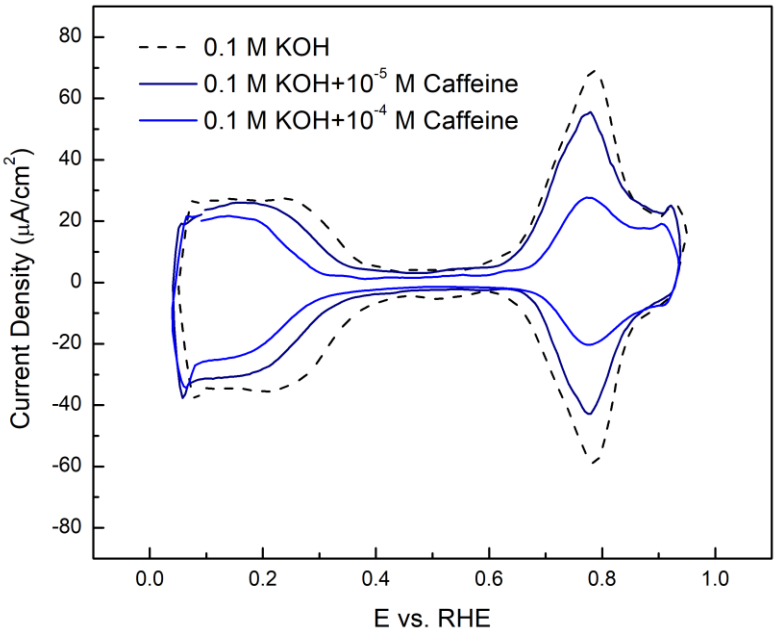

b)

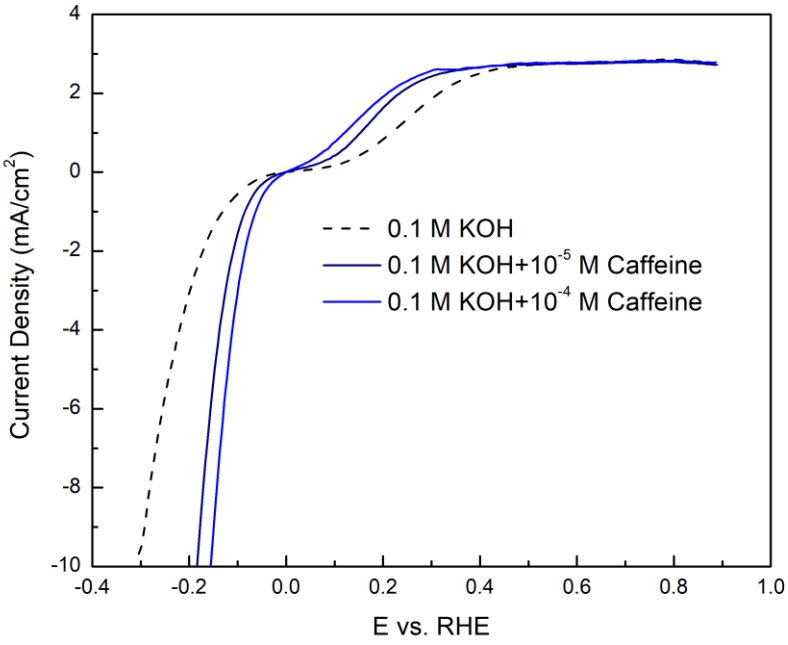

Figure S1: a) CVs and b) HER/HOR polarization curves of Pt (111) in 0.1 M KOH with: no caffeine, 10^{-5} M caffeine and 10^{-4} M caffeine at a scan rate of 50 mV/s.

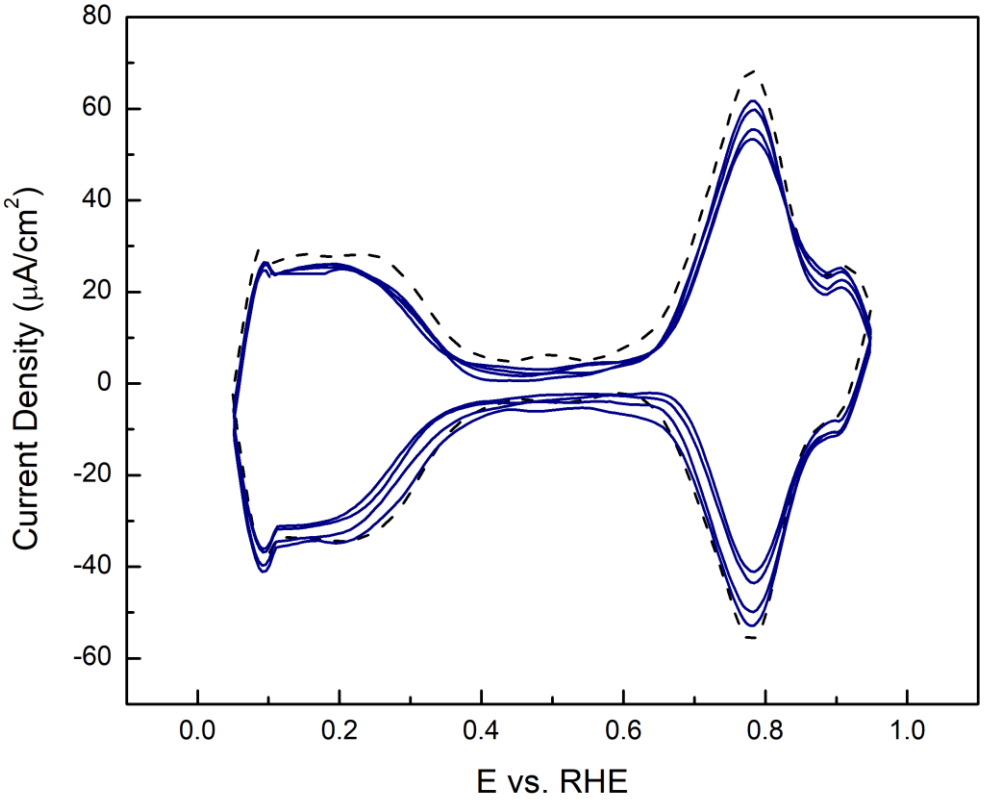

Figure S2: Gradual decay in H_{UPD} and OH_{ad} on Pt (111) with potential cycling in 0.1 M KOH + 10^{-5} M caffeine at a scan rate of 50 mV/s.

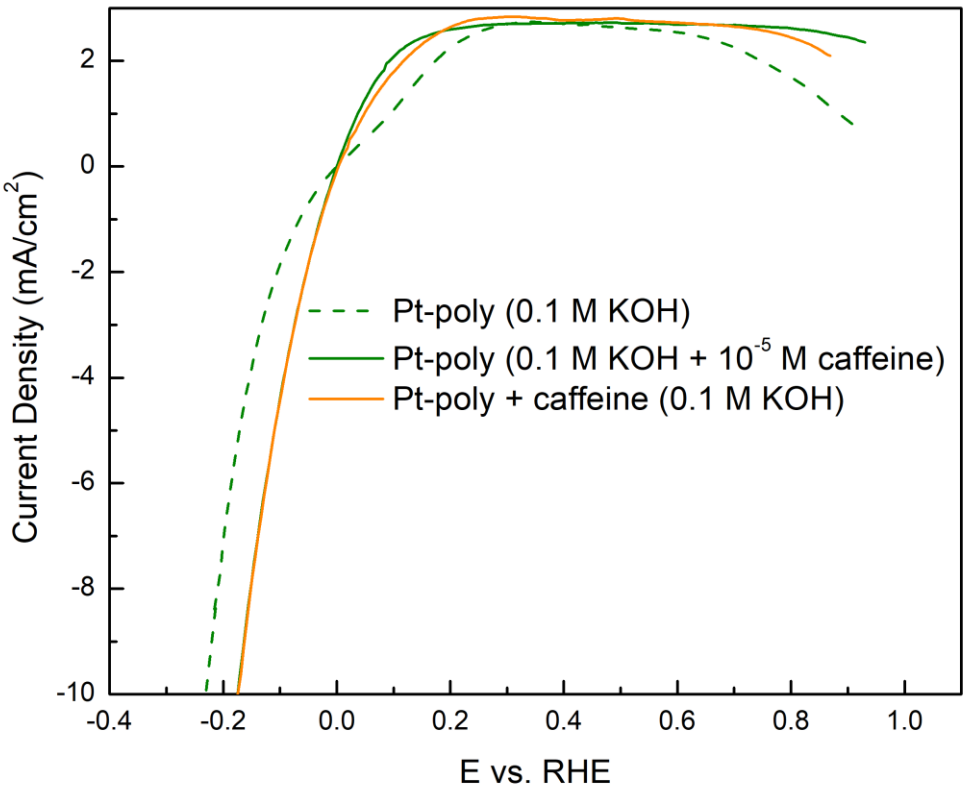

Figure S3: HER/HOR polarization curves at a scan rate of 50 mV/s of Pt-poly in H_2 purged 0.1 M KOH with: no caffeine (dashed green); 10^{-5} M caffeine (solid green) and Pt-poly + caffeine with no caffeine in solution (solid orange).

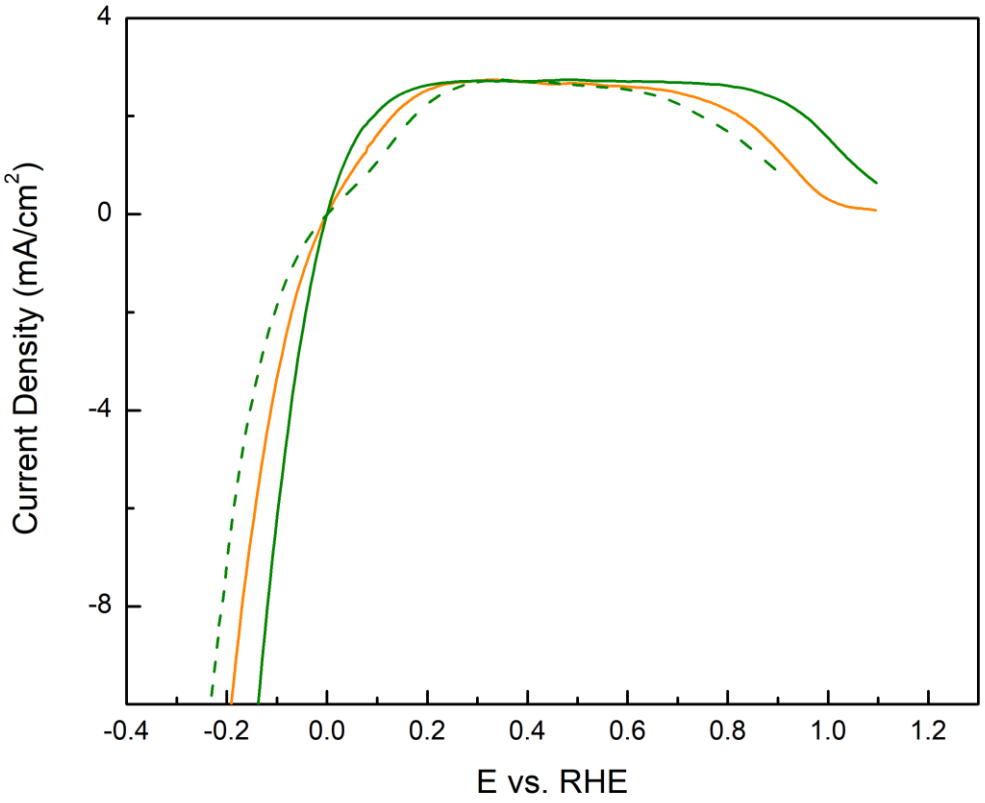

Figure S4: HER/HOR polarization curves at a scan rate of 50 mV/s of Pt-poly in H_2 purged 0.1 M KOH with: no caffeine (dashed green); 10^{-5} M caffeine (solid green) and Pt-poly + caffeine with no caffeine in solution (solid orange).

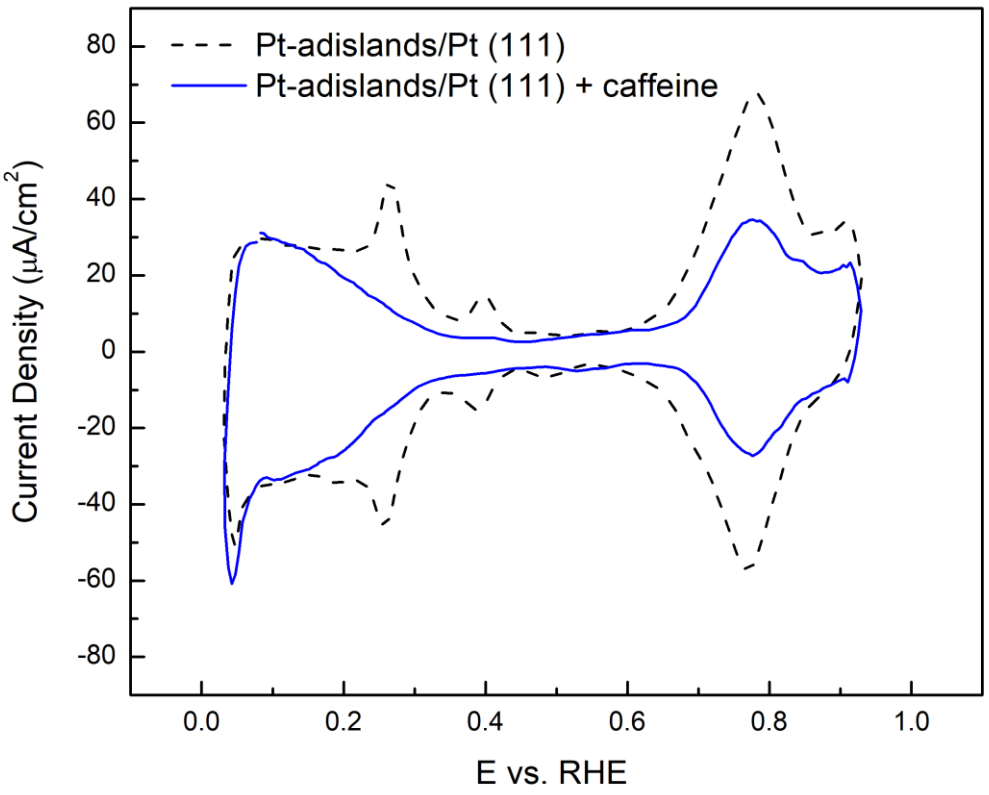

Figure S5: CV of Pt (111) + Pt adislands in Ar purged 0.1 M KOH at 50 mV/s with no caffeine and 10^{-5} M caffeine.

a)

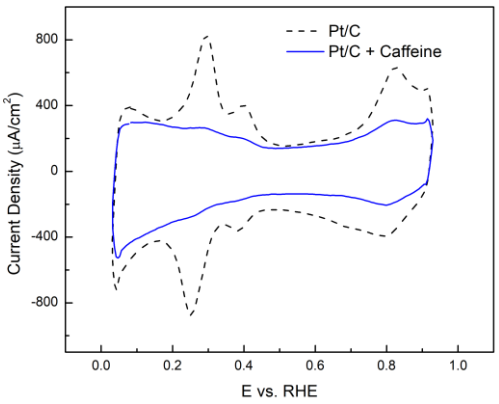

b)

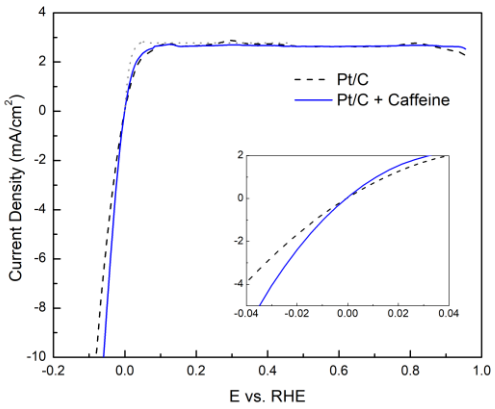

c)

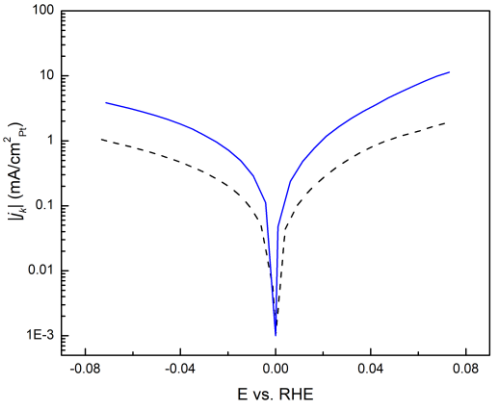

Figure S6: (a) CVs; (b) HER/HOR polarization curves (anodic sweep, scan rate: 20 mV/s); (c) Tafel plot of HER/HOR polarization curve for 40 wt% commercial Pt/C (Pt loading: 15 μg/cm^2) with caffeine (solid blue) and without caffeine (dashed black)

a)

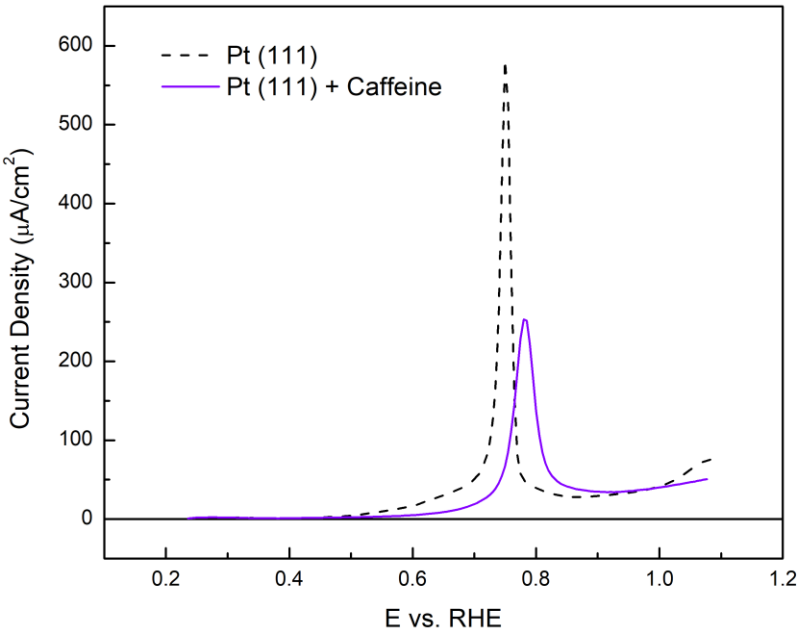

b)

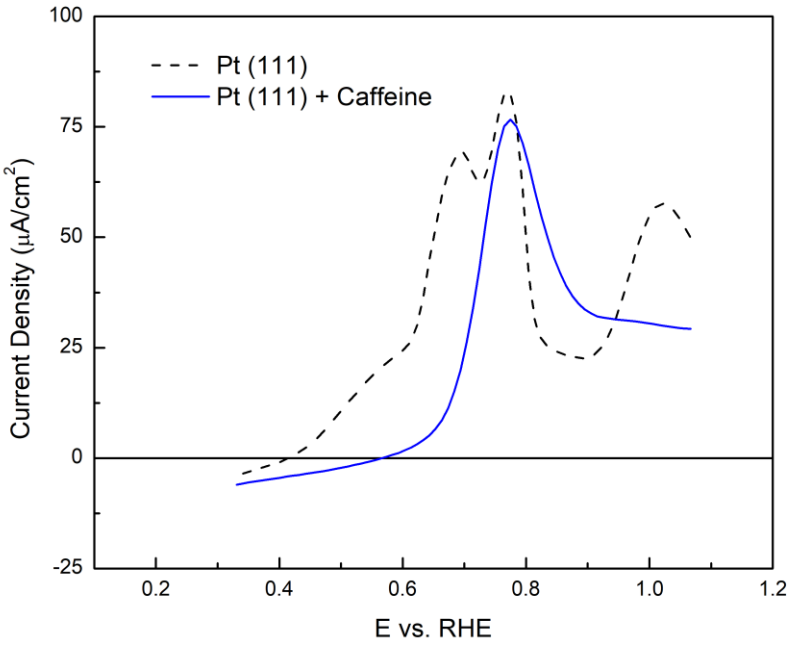

Figure S7: CO stripping curve of Pt (111) in Ar purged (a) 0.1 M $HClO_4$ and (b) 0.1 M KOH (no caffeine in electrolyte) at a scan rate of 50 mV/s.

a)

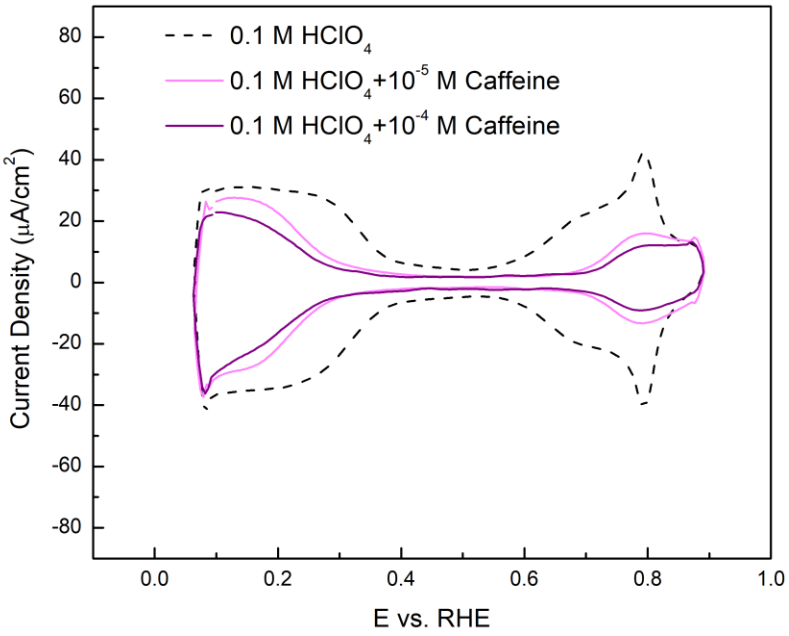

b)

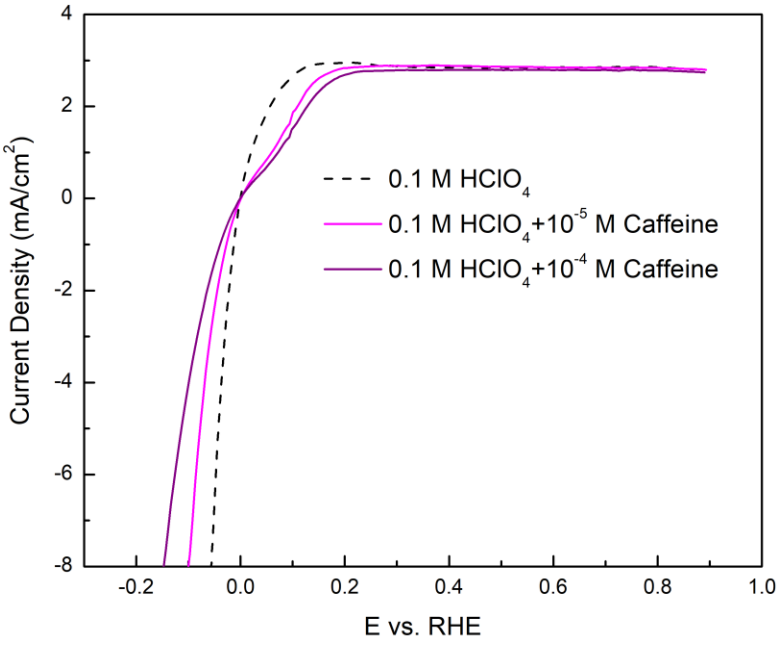

Figure S8: a) CVs and b) HER/HOR polarization curves of Pt (111) in 0.1 M $HClO_4$ with: no caffeine, 10^{-5} M caffeine and 10^{-4} M caffeine at a scan rate of 50 mV/s.

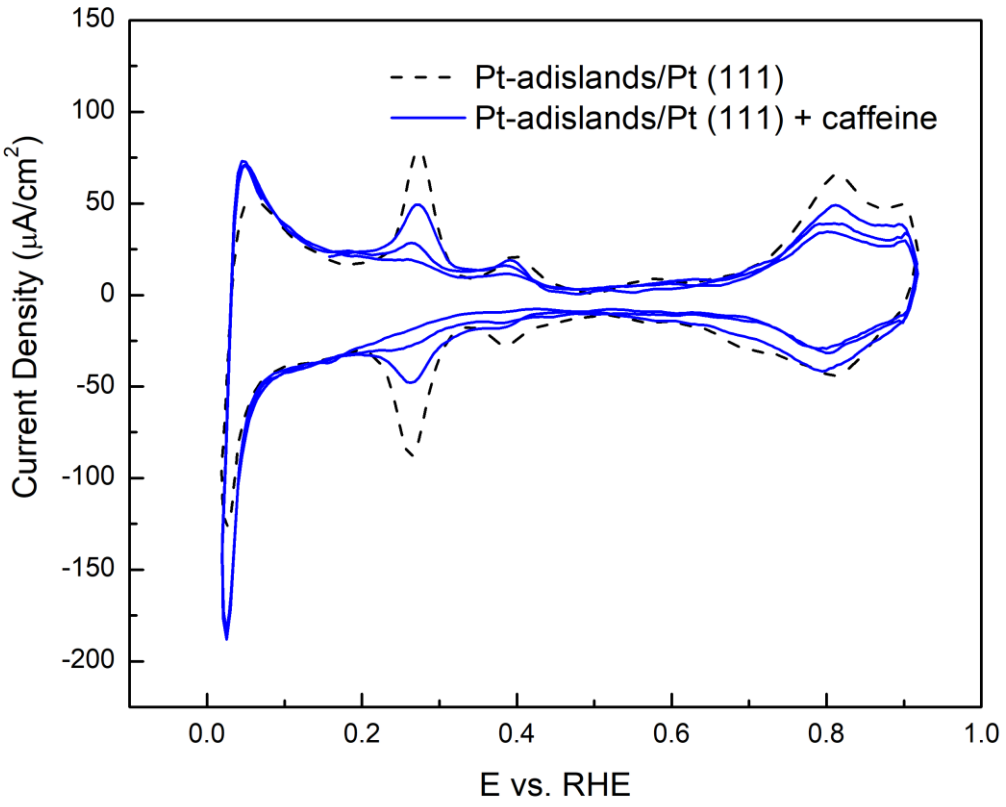

Figure S9: CV of Pt (111) + Pt adislands (high coverage) in Ar purged 0.1 M KOH at 50 mV/s with no caffeine and 10^{-5} M caffeine. CV shows the slow suppression of CV features with each subsequent cycle.

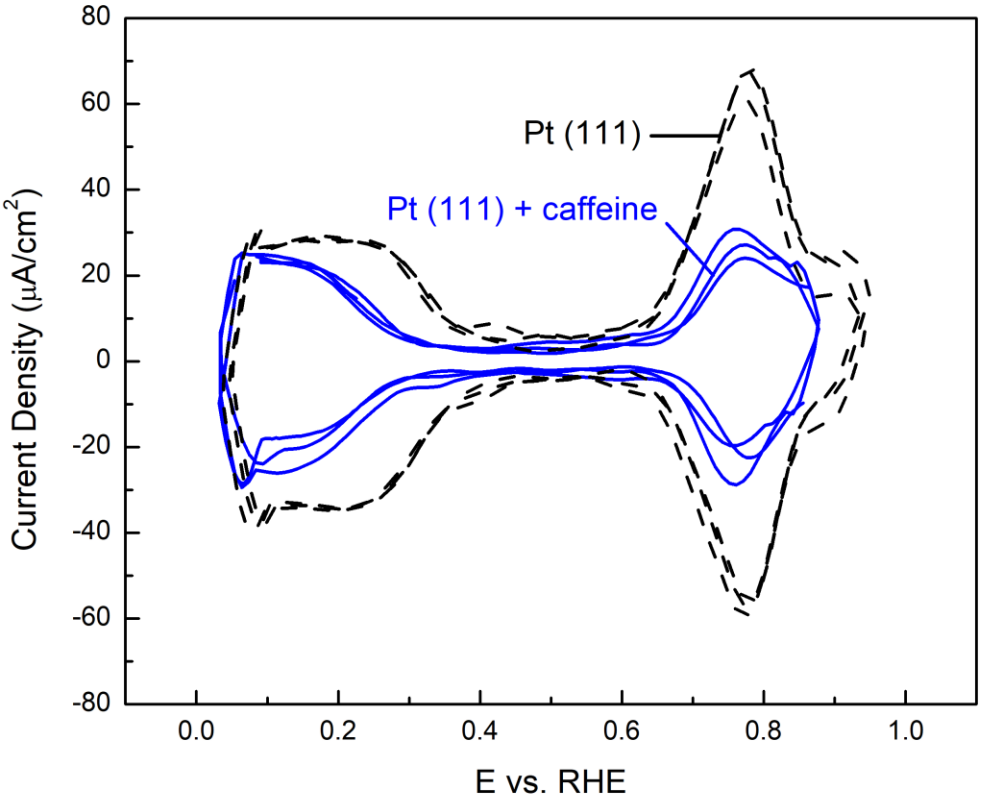

Figure S10: Reproducibility of cyclic voltammograms of Pt (111) in 0.1 M KOH

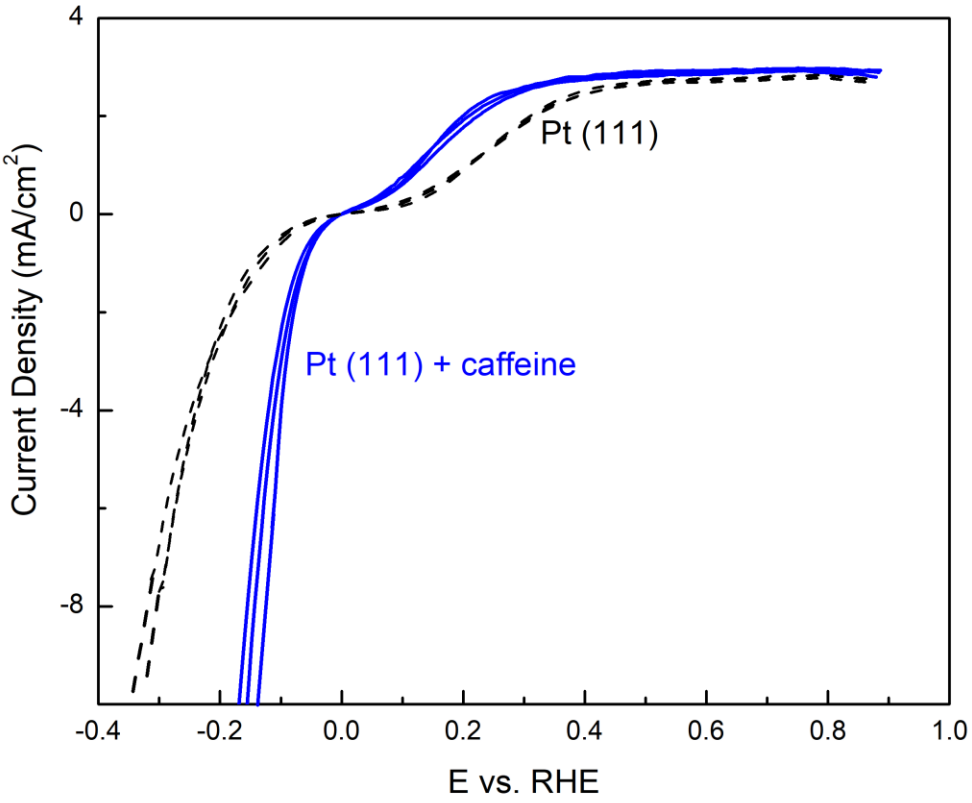

Figure S11: Reproducibility of HER-HOR polarization curves of Pt (111) in 0.1 M KOH

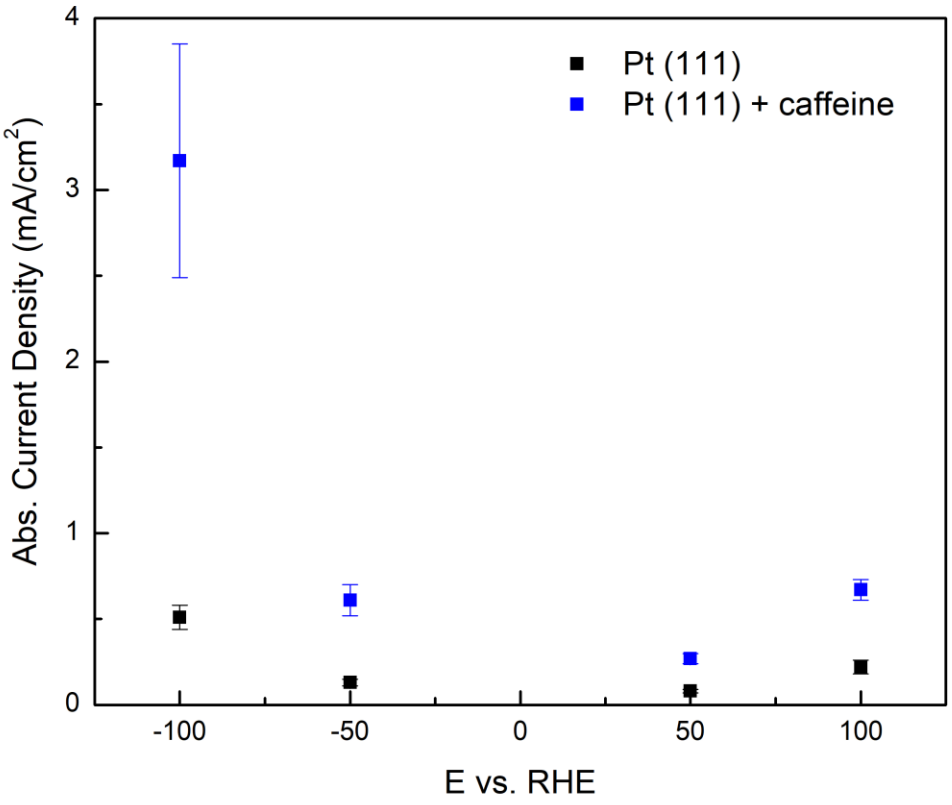

Figure S12: Absolute current densities for Pt (111) and Pt (111) + caffeine at various potentials in 0.1 M KOH with error bars.

a)

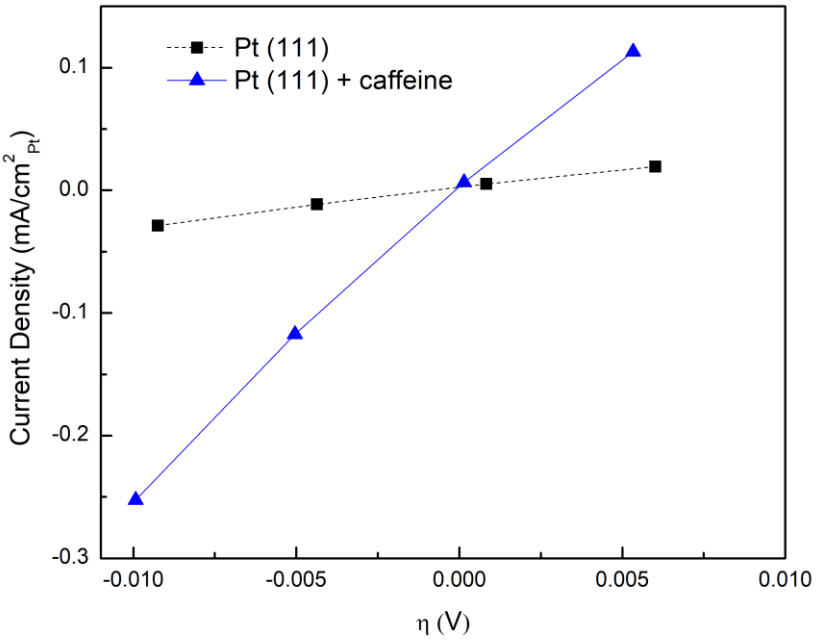

b)

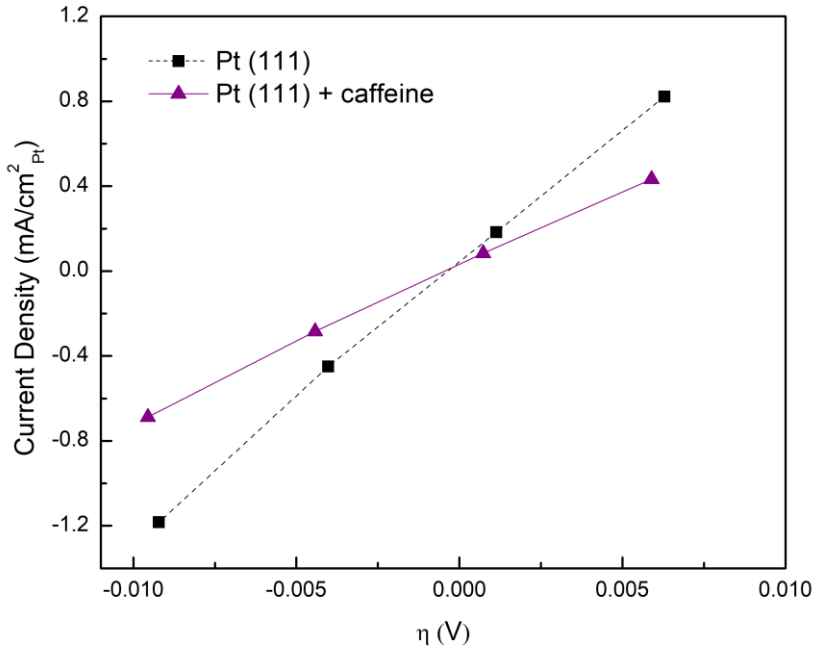

Figure S13: Low overpotential kinetic current density (normalized by Pt ECSA determined by H_{UPD}) in H_2 saturated (a) 0.1 M KOH and (b) 0.1 M $HClO_4$. Exchange current density is equal to the slope of the lines multiplied by RT/F, where F is Faraday's constant, R is the ideal gas constant, and T is temperature.

a)

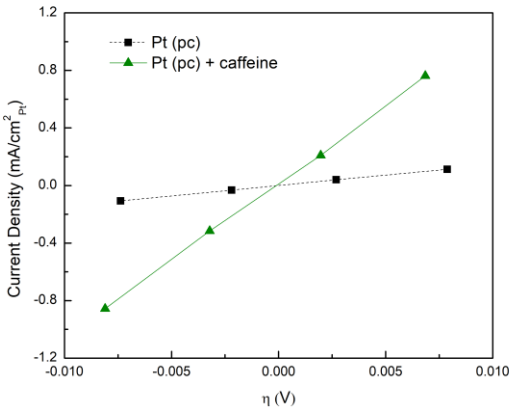

b)

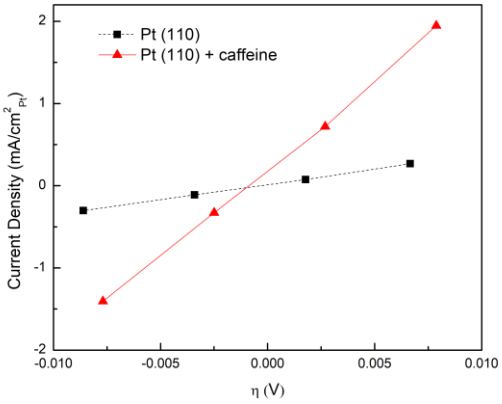

c)

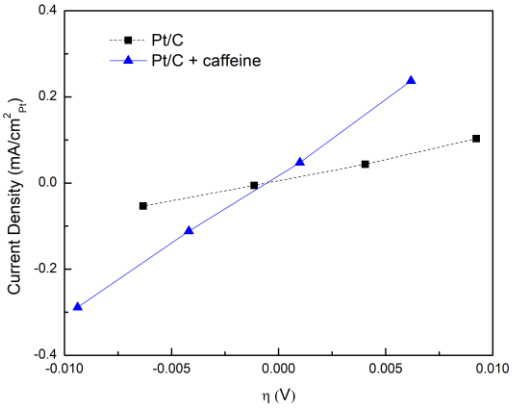

Figure S14: Low overpotential kinetic current density (normalized by Pt ECSA) in H_2 saturated 0.1 M KOH for (a) Pt (pc) ; (b) Pt (110) and (c) Pt/C. Exchange current density is equal to the slope of the lines multiplied by RT/F, where F is Faraday's constant, R is the ideal gas constant, and T is temperature.